

Local integrals of motion in dipole-conserving models with Hilbert space fragmentation

Patrycja Lydźba,¹ Peter Prelovšek,² and Marcin Mierzejewski¹

¹*Institute of Theoretical Physics, Wrocław University of Science and Technology, 50-370 Wrocław, Poland*

²*Department of Theoretical Physics, J. Stefan Institute, SI-1000 Ljubljana, Slovenia*

Hilbert space fragmentation is an ergodicity breaking phenomenon, in which Hamiltonian shatters into exponentially many dynamically disconnected sectors. In many fragmented systems, these sectors can be labelled by statistically localized integrals of motion, which are *nonlocal* operators. We study the paradigmatic nearest-neighbor pair hopping (PH) model exhibiting the so-called strong fragmentation. We show that this model hosts *local* integrals of motion (LIOMs), which correspond to frozen density modes with long wavelengths. The latter modes become subdiffusive when longer-range pair hoppings are allowed. Finally, we make a connection with a tilted (Stark) chain. Contrary to the dipole-conserving effective models, the tilted chain is shown to support either Hamiltonian or dipole moment as an LIOM. Numerical results are obtained from a numerical algorithm, in which finding LIOMs is reduced to the data compression problem.

Introduction.—Over the last two decades, a considerable effort has been made to understand whether an isolated quantum system thermalizes after being driven out of equilibrium. The thermal state is determined by just a few local integrals of motion (LIOMs) usually corresponding to conservations of energy and particle number. Moreover, their long-wavelength excitations, i.e., energy and density modes, attenuate according to the Fick’s law of diffusion [1]. It has been confirmed, also experimentally [2–4], that interacting systems typically thermalize. This is mostly understood in terms of the eigenstate thermalization hypothesis (ETH) [5–7].

It is natural to look for interacting systems that fail to thermalize. The most studied examples are integrable systems [8–11], which have *an extensive number* of LIOMs. These local (or quasilocal [12]) conserved operators affect the dynamics of other local observables. Specifically, the steady-state expectation values of local observables follow the predictions of the generalized Gibbs ensemble [13–17], which is set by the LIOMs. Additionally, LIOMs pose limits on the decay (in time) of correlation functions via the Mazur bound [18–20]. The inverse relation also holds, and the non-vanishing correlations at infinite time imply the existence of local or quasilocal integrals of motion [21].

More exotic violations of the ETH are also studied, such as the many-body localization (MBL). This phenomenon may arise from the intricate interplay of disorder and interactions that leads to emergent LIOMs, known as *l*-bits [22, 23]. We note that the existence of strict MBL in macroscopic systems is currently a subject of debate [24–28]. Similar physics has been proposed for Stark systems [29–33], in which the role of disorder is taken over by tilted potential. In the large tilt limit, its non-equilibrium dynamics is well captured by the effective models that strictly conserve the dipole moment [34–36]. The simplest one is the PH model that exhibits the Hilbert space fragmentation [37–43], since its Hamiltonian shatters into exponentially many blocks (Krylov subspaces) in the site occupation basis. We emphasize

that an important step towards understanding this phenomenon is the introduction of statistically localized integrals of motion [44, 45], which label the Krylov subspaces. Nevertheless, these are highly nonlocal operators and in general it is not obvious how nonlocal conserved operators affect the dynamics of local observables.

Since the presence of restrictions on the asymptotic dynamics of local observables is commonly understood as a manifestation of LIOMs, in this Letter we look for a connection between the Hilbert space fragmentation and their existence. First, we propose a numerical algorithm that establishes all LIOMs linear in a given set of operators. We employ it to demonstrate that the long wavelength density modes in the PH model are frozen and become strict LIOMs in the thermodynamic limit. Next, we argue that these density modes become subdiffusive after incorporating longer-range pair hoppings to the PH model, which break the strong fragmentation. Finally, we make a connection with the full Stark model. We demonstrate that although both energy and dipole moment are conserved in the thermodynamic limit [46], they correspond to a single LIOM in this case.

Method.—We first develop a simple algorithm that determines whether and how many LIOMs can be constructed from a fixed set of operators. We consider a Hilbert space of dimension Z , which is spanned by energy eigenstates, $H|n\rangle = E_n|n\rangle$, and denote matrix elements of observables as $A_{mn} = \langle m|A|n\rangle$. We are interested in Hermitian operators, for which the Hilbert-Schmidt (HS) product is

$$\langle AB \rangle = \frac{1}{Z} \text{Tr}(AB) = \frac{1}{Z} \sum_{m,n} A_{mn} B_{mn}^* \quad (1)$$

and the HS norm is $\|A\|^2 = \langle AA \rangle = 1/Z \sum_{m,n} |A_{mn}|^2$.

Considering an arbitrary set of orthonormal operators, $\langle A^i A^{i'} \rangle = \delta_{ii'}$, we construct the orthogonal transformation

$$B^\beta = \sum_i \mathcal{V}_{i\beta} A^i, \quad (2)$$

so that the set $\{B^\beta\}$ includes all LIOMs linear in A^i . If the set $\{A^i\}$ contains only local observables then all generated B^β are local by construction. We note that local observables are the ones that can be written as sums of operators involving a finite number of sites, i.e., having a finite support. From now on, we explicitly distinguish LIOMs from other operators using the symbol Q^β (\mathcal{B}^β) for B^β that do (do not) commute with the Hamiltonian. Moreover, we work in the Hilbert space with a fixed particle number N . Since N is trivially conserved, we do not discuss it or explicitly include in the set of LIOMs.

In order to find LIOMs, we use the infinite time averaging

$$\bar{A} = \lim_{\tau \rightarrow \infty} \frac{1}{\tau} \int_0^\tau e^{iHt} A e^{-iHt} dt = \sum_{\substack{m,n \\ E_n = E_m}} A_{nm} |n\rangle \langle m|. \quad (3)$$

It is evident that the time averaging does not modify LIOMs ($\bar{Q}^\beta = Q^\beta$), while it eliminates some of the matrix elements of \mathcal{B}^β ($\bar{\mathcal{B}}_{mn}^\beta = 0$ for $E_m \neq E_n$). Therefore, LIOMs can be singled out just by examining the norms of the time-averaged operators, $\|\bar{Q}^\beta\|^2 = 1$ whereas $\|\bar{\mathcal{B}}^\beta\|^2 < 1$.

We note that the nonergodic behavior of the observables A^i is encoded in the matrix elements of \bar{A}^i . We store all matrix elements of all \bar{A}^i in a single matrix \mathcal{R} so that its i -th column contains A_{mn}^i for $E_m = E_n$. In Supplemental Material [47], we demonstrate that LIOMs can be established from the compression of data stored in \mathcal{R} . Such compression can be achieved via singular value decomposition, $\mathcal{R} = U \Sigma \mathcal{V}^T$, where the diagonal matrix $\Sigma = \text{diag}(\tilde{\lambda}_1, \tilde{\lambda}_2, \dots)$ stores the singular values and the orthogonal matrix \mathcal{V} is the same as in Eq. (2). According to the Eckart–Young–Mirsky theorem, the compression amounts to the approximation $\mathcal{R} \simeq \mathcal{R}^\parallel = U \Sigma^\parallel \mathcal{V}^T$, where Σ^\parallel contains only the largest $\tilde{\lambda}_\beta$. We consider positive $\tilde{\lambda}_\beta$ sorted in descending order, and introduce notation $\lambda_\beta = \tilde{\lambda}_\beta^2 / Z$. In Ref. [47], we show that the HS norms of the time-averaged operators from Eq. (2) read $\|\bar{B}^\beta\|^2 = \lambda_\beta \leq 1$. Based on the arguments from the preceding paragraph, we note that the largest $\lambda_\beta = 1$ define LIOMs, i.e., $Q^\beta = \bar{B}^\beta = B^\beta$.

Pair hopping model.—We use the introduced method to investigate LIOMs in the simplest effective model for the tilted chain. Namely, we consider the PH model with L sites and $N = L/2$ spinless fermions [36],

$$H_1 = \sum_{i=1}^{L-3} (c_i^\dagger c_{i+3}^\dagger c_{i+2} c_{i+1} + \text{H.c.}). \quad (4)$$

Here, c_i^\dagger (c_i) creates (annihilates) a spinless fermion at site i , and we define a traceless site occupation as $n_i = c_i^\dagger c_i - N/L$. This model conserves the dipole moment $M = \sum_i i n_i$ as well as the sublattice particle numbers $n_{\text{even}} = \sum_{i \in \text{even}} n_i$ and $n_{\text{odd}} = N - n_{\text{even}}$.

The PH model manifests the strong fragmentation, so that the size of the largest Krylov subspace is ex-

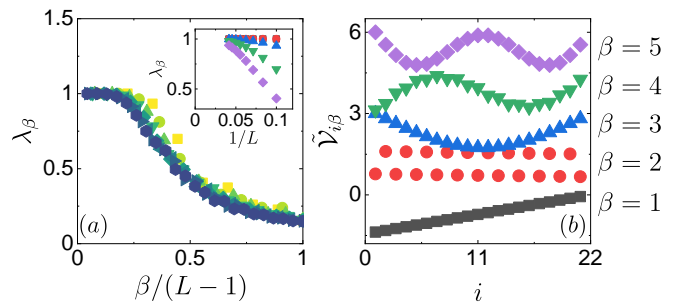


FIG. 1. \bar{B}^β established from $A^i \in \mathcal{N}$ for the PH model from Eq. (4). (a) The HS norms λ_β as functions of $\beta/(L-1)$. We consider $L = 10, \dots, 24$ and darker colors represent larger systems. The inset shows the finite size scaling of the five largest λ_β . (b) Components of the rotated operator, $\tilde{V}_{i\beta}$, for the five largest λ_β and $L = 22$. Colors are consistent with the inset in (a). For clarity, we shift the curves for various β along the vertical axis, i.e., $\tilde{V}_{i\beta} \rightarrow \tilde{V}_{i\beta} + 1.5(\beta - 1)$.

ponentially smaller than the dimension of the Hilbert space Z [36, 48]. While the existence of blocks appears to affect the non-equilibrium dynamics leading to the lack of thermalization [43], it remains unclear whether it is linked to the existence of local (or quasilocal) LIOMs [21, 49]. Recall that the latter are different than the statistically localized integrals of motion introduced in [44, 45]. Moreover, the density modes are expected to undergo a subdiffusive relaxation, in agreement with the fracton hydrodynamics [50–53], only after longer-range pair hoppings are included in the model (see [54, 55] for results in classical circuit models). Below, we demonstrate that establishing LIOMs helps to understand these features.

It has been argued in Ref. [43] that the density-density correlations $\langle n_i(t) n_i \rangle$ do not decay to zero at long times in the PH model. Therefore, it is straightforward to look for LIOMs that are linear combinations of n_i . We emphasize that in the subspace with a fixed number of particles, n_i are neither independent ($\sum_{i=1}^L n_i = 0$) nor orthogonal ($\langle n_i n_j \rangle \neq \delta_{ij}$). Hence, we select the set of independent occupations $\{n_i\}$ with $i \leq L-1$, which we then orthogonalize, $\sum_{j,k=1}^{L-1} U_{aj} \langle n_j n_k \rangle U_{kb}^T = \delta_{ab} \sigma_a$, to obtain the set \mathcal{N} of orthonormal operators $A^a = \sum_{i=1}^{L-1} \frac{1}{\sqrt{\sigma_a}} U_{ia} n_i$ [47]. Nevertheless, one can still express B^β from Eq. (2) as linear combinations of occupations, $B^\beta = \sum_{a=1}^{L-1} \mathcal{V}_{a\beta} A^a = \sum_{a,i=1}^{L-1} \frac{1}{\sqrt{\sigma_a}} \mathcal{V}_{a\beta} U_{ia} n_i = \sum_{i=1}^{L-1} \tilde{V}_{i\beta} n_i$.

Results for λ_β are shown in Fig. 1(a). Simultaneously in Fig. 1(b), we plot the coefficients $\tilde{V}_{i\beta}$ shifted along the vertical axis for clarity, i.e., $\tilde{V}_{i\beta} \rightarrow \tilde{V}_{i\beta} + 1.5(\beta - 1)$. We find that $\lambda_1 = \lambda_2 = 1$ for all system sizes, and that they correspond to the dipole moment M (see black squares in Fig. 1(b)) and the sublattice particle number n_{even} (see red circles in Fig. 1(b)). The other λ_β within the plateau in Fig. 1(a), i.e., for $\beta \geq 3$, appear to increase towards one with a system size, as demonstrated in the inset of

Fig. 1(a). Consequently, there are infinitely many many LIOMs in the thermodynamic limit. Although we are not able to determine from Fig. 1(a) whether their number is linear or sublinear in L , their presence explains the previously reported lack of thermalization (see [18–20]). We therefore expect that the conventional measures of quantum chaos will be similar to the ones of integrable systems (see [56–58]). For the example of spectral statistics see Supplemental Material [47].

It is worth to highlight that Q^β within the plateau in Fig. 1(a) with $\beta \geq 3$ correspond to density modes with wave vectors $q = \frac{(\beta-2)\pi}{L}$, which are slightly distorted to ensure orthogonality. The HS norm $\|\bar{Q}^\beta\| = 1$ means that Q^β does not have any off-diagonal matrix elements in the energy basis, so that it cannot show any dynamics at any time scale. Therefore, these density modes are strictly frozen in the thermodynamic limit. In the following, we show that longer-range pair hoppings added to H_1 unfreeze the density modes and restore the fracton hydrodynamics.

Extended pair hopping model.—It has been demonstrated that including longer-range pair hoppings in the PH model changes the fragmentation from strong to weak, so that the dimension of the largest block becomes a finite fraction of the total number of states Z [38]. The resulting Hamiltonian supports the weak ETH, in which the majority of eigenstates is thermal but nonthermal outliers (dubbed many-body scars) are allowed [39].

It is reasonable to expect that the number of LIOMs decreases when the fragmentation becomes weak. We verify this expectation by studying the extended pair hopping (EPH) model with two additional terms

$$H_2 = H_1 + \sum_{i=1}^{L-4} (c_i^\dagger c_{i+4}^\dagger c_{i+3} c_{i+1} + \text{h.c.}) + \sum_{i=1}^{L-5} (c_i^\dagger c_{i+5}^\dagger c_{i+4} c_{i+1} + \text{h.c.}). \quad (5)$$

We stress that H_2 in Eq. (5) no longer commutes with the sublattice particle numbers n_{even} or n_{odd} . The same Hamiltonian but without the last term is studied in the Supplemental Material [47]. It yields similar results to those discussed below, however, the finite-size scaling does not provide a clear picture of the thermodynamic limit. In the Supplemental Material [47], we also provide the derivation starting from the tilted chain that generates all dipole-conserving terms, as the ones from Eq. (5). Nevertheless, the actual parameters in Eq. (5) are settled to one and, so, are not meant to represent a realistic effective model of the tilted chain.

In Fig. 2(a), we show the HS norms λ_β , where B^β are linear combinations of occupations, $A^i \in \mathcal{N}$. It is clear from the inset of Fig. 2(a) that only λ_1 is equal to one for all system sizes. It corresponds to the dipole moment M (not shown). Simultaneously, all other λ_β decrease to zero with a system size. They correspond to the same density modes as shown in Fig. 1(b).

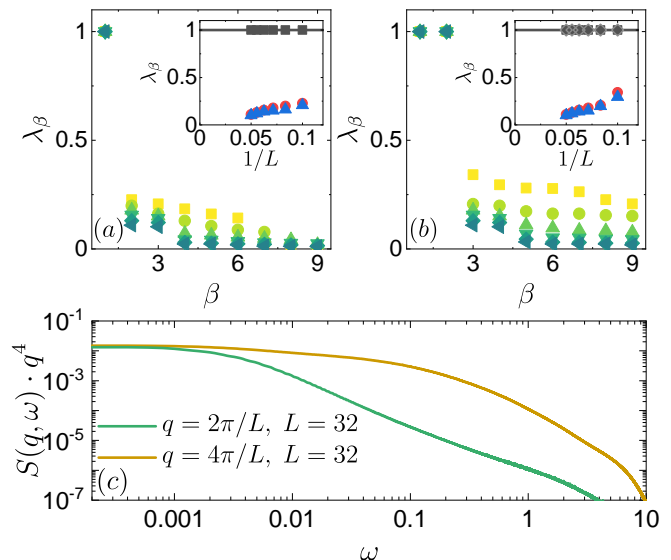


FIG. 2. (a,b) The same as in Fig. 1(a) but for the EPH model from Eq. (5), $\beta \leq 9$ and $L = 10, \dots, 20$. Results were obtained for various sets of operators: (a) $A^i \in \mathcal{N}$, (b) $A^i \in \mathcal{N}_{2E}$. (c) The dynamical structure factor $S(q, \omega)$ for two smallest $q = 2\pi/L, 4\pi/L$.

The set of operators that we have considered so far, \mathcal{N} , does not allow to construct the Hamiltonian as an independent LIOM orthogonal to other LIOMs. Therefore, we also study an extended set, \mathcal{N}_{2E} , which includes all operators from \mathcal{N} as well as the pair hopping terms, $c_i^\dagger c_{i+3}^\dagger c_{i+2} c_{i+1} + \text{H.c.}$, $c_i^\dagger c_{i+4}^\dagger c_{i+3} c_{i+1} + \text{H.c.}$ and $c_i^\dagger c_{i+5}^\dagger c_{i+4} c_{i+1} + \text{H.c.}$ Note that i runs through all values for which the site indexes do not exceed L . Numerical results obtained for $A^i \in \mathcal{N}_{2E}$ confirm that the Hamiltonian from Eq. (5) supports only two independent conservation laws, as visible in Fig. 2(b). The first LIOM is the dipole moment M , while the second LIOM is the Hamiltonian H_2 .

We now confirm that the density modes relax subdiffusively within the EPH model. Specifically, we numerically calculate the dynamical structure factor $S(q, \omega)$, i.e., the dynamical correlation function for density modulations $n_q = 1/\sqrt{L} \sum_i \cos(q(i - L/2)) n_i$ in the infinite-temperature limit, employing the microcanonical Lanczos method [59, 60]. More details can be found in [47]. In the hydrodynamic regime $q \ll 1$, the density modulations should exhibit a slow decay with a characteristic rate Γ_q , so that the low $\omega \ll 1$ correlations should behave as $\pi S(q, \omega) \sim \chi^0 \Gamma_q / (\omega^2 + \Gamma_q^2)$ with the corresponding susceptibility $\chi^0 = (1/2)\bar{n}(1 - \bar{n})$ and the average density $\bar{n} = 1/2$. We plot results for two smallest $q = 2\pi/L, 4\pi/L$ in Fig. 2(c), and we find that the relaxation rates scale as $\Gamma_q \propto q^4$, as required for the subdiffusion.

Stark model.—Since the Hamiltonians in Eqs. (4) and (5) arise as effective models for the strongly tilted

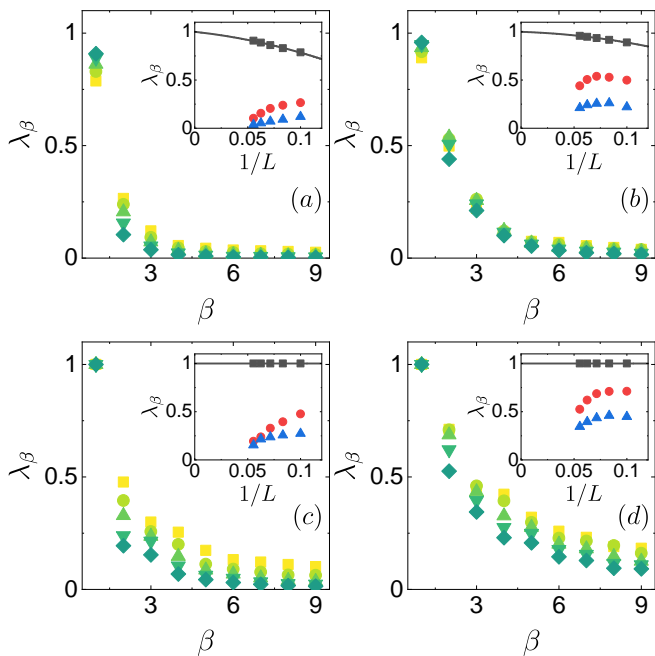


FIG. 3. The same as in Figs. 2(a) and 2(b) but for the Stark chain from Eq. (6), $\beta \leq 9$ and $L = 10, \dots, 18$. Results in different columns were obtained for different fields: (a,c) $F = 1.0$, (b,d) $F = 1.5$. Results in different rows were obtained for different sets of operators: (a,b) $A^i \in \mathcal{N}$, (c,d) $A^i \in \mathcal{N}_{3E}$. The solid lines are the second-order polynomial fits to data, serving as guides for the eye.

chain [36, 47],

$$H_3 = t \sum_{i=1}^{L-1} (c_i^\dagger c_{i+1} + \text{h.c.}) + FM + V \sum_{i=1}^{L-1} n_i n_{i+1}, \quad (6)$$

it is instructive to establish LIOMs also in the latter system. We show that the set of LIOMs in the Stark model differs from the two cases considered earlier. Note that F is the strength of the tilt. Throughout the paper, we fix the hopping integral and the interaction strength to $t = 1$ and $V = 2$, respectively. For convenience, we denote the translationally invariant part of the Hamiltonian as $H_3^{(0)} = H_3 - FM$.

The nonequilibrium dynamics of the Stark model has been previously explained in terms of the (approximate) Hilbert space shattering, and the many-body localization in the thermodynamic limit has been proposed [30, 33]. Nevertheless, its transport properties are captured by the PH model only in small systems and large fields [36]. Moreover, it has been recently argued that the dipole moment M is conserved in the thermodynamic limit and the density profiles undergo subdiffusive dynamics [46] (see also [61, 62]). This is consistent with our numerical results. In Fig. 3(a) and 3(b), we demonstrate the HS norm λ_β for B^β that are linear in $A^i \in \mathcal{N}$ for fields $F = 1.0$ and 1.5 , respectively. Only λ_1 increases towards one with a system size, and it corresponds to the

dipole moment M . The other λ_β with $\beta \geq 2$ decrease for $L \geq L^*$. They correspond to the density modes from Fig. 1(b). We find that L^* depends on F , so that it exceeds the maximal system size available in our numerical simulations for $F \gtrsim 2$. This causes the density modes to appear frozen in finite systems.

We note that the derivation of the dipole moment conservation from [46] is based on the scaling of the HS norms $\|H_3^{(0)}\|^2 \propto L$ and $\|M\|^2 \propto L^3$ together with the orthogonality $\langle H_3^{(0)} M \rangle = 0$. This brings into question, whether the dipole moment M gives rise to an LIOM independent of H_3 or it simply becomes H_3 in the thermodynamic limit. The mere fact that M and H_3 are conserved does not imply that their difference $H_3^{(0)} = H_3 - FM$ is also an LIOM. Moreover, the vanishing ratio of norms $\|\bar{H}_3^{(0)}\|/\|H_3\| \leq \mathcal{O}(1/L)$ does not exclude that $H_3^{(0)}$ is an LIOM. We emphasize that conserved quantities restrict the relaxation of observables via the Mazur bound [18–20], which involves *normalized* LIOMs. Therefore, the significance of $H_3^{(0)}$ for the relaxation of observables depends on the ratio $\|\bar{H}_3^{(0)}\|/\|H_3^{(0)}\|$.

For this reason, we complement the study by looking for Q^β that are linear in $A^i \in \mathcal{N}_{3E}$, where the set \mathcal{N}_{3E} includes all operators from \mathcal{N} as well as the nearest-neighbor interactions $n_i n_{i+1}$ and hoppings $c_{i+1}^\dagger c_i + \text{h.c.}$ for $i = 1, \dots, L-1$. Note that every term in the Hamiltonian from Eq. (6) belongs to \mathcal{N}_{3E} . Figures 3(c) and 3(d) reveal an important difference between the Stark chain and the effective model, shown in Fig. 2(b). In the latter case, the Hamiltonian and dipole moment are two orthogonal LIOMs. In contrast to this, both form only a single LIOM in the Stark chain (in addition to the particle number conservation). When extending the sets of operators from \mathcal{N} to \mathcal{N}_{3E} , the dipole moment M is replaced by the Hamiltonian H_3 . Therefore, the conservation of dipole moment is not independent from the conservation of energy.

Identification of the conservation laws is the starting point for constructing the relevant hydrodynamics. Our results indicate that in the case of the EPH model one should account for the conservation of the particle number, dipole moment and energy [51, 52]. On the other hand, for the tilted Hamiltonian H_3 one should use either the energy conservation or the dipole moment conservation [46, 61], as these two conservation laws are equivalent in the thermodynamic limit.

Summary.—In this Letter, we have studied the PH model, which is a paradigmatic model of the Hilbert space fragmentation, and arises in the Schrieffer-Wolff transformation of the Stark model. First, we have put forward a numerical algorithm based on the data compression problem, which generates all LIOMs linear in a given set of operators. Next, we have established that the PH model hosts an infinite number number of LIOMs in the thermodynamic limit. While the PH model is translationally invariant, the obtained LIOMs are not. They

correspond to frozen density modes excluding any particle hydrodynamics. On the other hand, density modes decay when longer-range pair hoppings are allowed and become subdiffusive in agreement with the fracton hydrodynamics.

We have also revealed an important difference between the Stark chain and its effective models. In the latter cases, the Hamiltonian and dipole moment are two orthogonal LIOMs. In contrast to this, they form only one LIOM in the tilted (Stark) chain.

ACKNOWLEDGMENTS

We acknowledge discussions with J. Herbrych, A. Głódkowski and L. Vidmar. We also acknowledge the support of the National Science Centre, Poland via projects 2023/07/X/ST3/01707 (P. Ł.) and 2020/37/B/ST3/00020 (M. M.) as well as the support of the Slovenian Research Agency via the program P1-0044 (P. P.). Numerical studies in this work have been partially carried out using resources provided by the Wrocław Centre for Networking and Supercomputing, Grant No. 579 (P. Ł.).

-
- [1] B. Bertini, F. Heidrich-Meisner, C. Karrasch, T. Prosen, R. Steinigeweg, and M. Žnidarič, Finite-temperature transport in one-dimensional quantum lattice models, *Rev. Mod. Phys.* **93**, 025003 (2021).
- [2] S. Trotzky, Y.-A. Chen, A. Flesch, I. P. McCulloch, U. Schollwöck, J. Eisert, and I. Bloch, Probing the relaxation towards equilibrium in an isolated strongly correlated one-dimensional Bose gas, *Nature Physics* **8**, 325–330 (2012).
- [3] A. M. Kaufman, M. E. Tai, A. Lukin, M. Rispoli, R. Schittko, P. M. Preiss, and M. Greiner, Quantum thermalization through entanglement in an isolated many-body system, *Science* **353**, 794–800 (2016).
- [4] G. Clos, D. Porras, U. Warring, and T. Schaetz, Time-resolved observation of thermalization in an isolated quantum system, *Phys. Rev. Lett.* **117**, 170401 (2016).
- [5] M. Srednicki, Chaos and quantum thermalization, *Phys. Rev. E* **50**, 888 (1994).
- [6] J. M. Deutsch, Eigenstate thermalization hypothesis, *Rep. Prog. Phys.* **81**, 082001 (2018).
- [7] L. D’Alessio, Y. Kafri, A. Polkovnikov, and M. Rigol, From quantum chaos and eigenstate thermalization to statistical mechanics and thermodynamics, *Adv. Phys.* **65**, 239 (2016).
- [8] Y. Tang, W. Kao, K.-Y. Li, S. Seo, K. Mallayya, M. Rigol, S. Gopalakrishnan, and B. L. Lev, Thermalization near integrability in a dipolar quantum newton’s cradle, *Phys. Rev. X* **8**, 021030 (2018).
- [9] T. Kinoshita, T. Wenger, and S. D. Weiss, A quantum Newton’s cradle, *Nature (London)* **440**, 900 (2006).
- [10] M. Rigol and M. Fitzpatrick, Initial-state dependence of the quench dynamics in integrable quantum systems, *Phys. Rev. A* **84**, 033640 (2011).
- [11] F. Franchini, *An Introduction to Integrable Techniques for One-Dimensional Quantum Systems* (Springer International Publishing, 2017).
- [12] T. Prosen, Open XXZ spin chain: Nonequilibrium steady state and a strict bound on ballistic transport, *Phys. Rev. Lett.* **106**, 217206 (2011).
- [13] M. Rigol, V. Dunjko, V. Yurovsky, and M. Olshanii, Relaxation in a completely integrable many-body quantum system: An ab initio study of the dynamics of the highly excited states of 1d lattice hard-core bosons, *Phys. Rev. Lett.* **98**, 050405 (2007).
- [14] L. Vidmar and M. Rigol, Generalized gibbs ensemble in integrable lattice models, *J. Stat. Mech.* **2016**, 064007 (2016).
- [15] T. Langen, S. Erne, R. Geiger, B. Rauer, T. Schweigler, M. Kuhnert, W. Rohringer, I. E. Mazets, T. Gasenzer, and J. Schmiedmayer, Experimental observation of a generalized gibbs ensemble, *Science* **348**, 207 (2015).
- [16] S. Ziraldo and G. E. Santoro, Relaxation and thermalization after a quantum quench: Why localization is important, *Phys. Rev. B* **87**, 064201 (2013).
- [17] P. Lydzba, M. Mierzejewski, M. Rigol, and L. Vidmar, Generalized thermalization in quantum-chaotic quadratic hamiltonians, *Phys. Rev. Lett.* **131**, 060401 (2023).
- [18] M. Suzuki, Ergodicity, constants of motion, and bounds for susceptibilities, *Physica* **51**, 277 (1971).
- [19] P. Mazur, Non-ergodicity of phase functions in certain systems, *Physica* **43**, 533 (1969).
- [20] X. Zotos, F. Naef, and P. Prelovsek, Transport and conservation laws, *Phys. Rev. B* **55**, 11029 (1997).
- [21] M. Mierzejewski and L. Vidmar, Quantitative impact of integrals of motion on the eigenstate thermalization hypothesis, *Phys. Rev. Lett.* **124**, 040603 (2020).
- [22] R. Nandkishore and D. A. Huse, Many-body localization and thermalization in quantum statistical mechanics, *Annu. Rev. Condens. Matter Phys.* **6**, 15 (2015).
- [23] D. A. Abanin, E. Altman, I. Bloch, and M. Serbyn, Colloquium: Many-body localization, thermalization, and entanglement, *Rev. Mod. Phys.* **91**, 021001 (2019).
- [24] J. Šuntajs, J. Bonča, T. Prosen, and L. Vidmar, Ergodicity breaking transition in finite disordered spin chains, *Phys. Rev. B* **102**, 064207 (2020).
- [25] J. Šuntajs, J. Bonča, T. Prosen, and L. Vidmar, Quantum chaos challenges many-body localization, *Phys. Rev. E* **102**, 062144 (2020).
- [26] T. LeBlond, D. Sels, A. Polkovnikov, and M. Rigol, Universality in the onset of quantum chaos in many-body systems, *Phys. Rev. B* **104**, L201117 (2021).
- [27] B. Krajewski, L. Vidmar, J. Bonča, and M. Mierzejewski, Strongly disordered Anderson insulator chains with generic two-body interaction, *Phys. Rev. B* **108**, 064203 (2023).
- [28] P. Prelovšek, J. Herbrych, and M. Mierzejewski, Slow diffusion and Thouless localization criterion in modulated spin chains, *Phys. Rev. B* **108**, 035106 (2023). 2302.03325.
- [29] E. van Nieuwenburg, Y. Baum, and G. Refael, From bloch oscillations to many-body localization in clean in-

- interacting systems, *Proc. Natl. Acad. Sci.* **116**, 9269–9274 (2019).
- [30] E. V. H. Doggen, I. V. Gornyi, and D. G. Polyakov, Stark many-body localization: Evidence for Hilbert-space shattering, *Phys. Rev. B* **103**, L100202 (2021).
- [31] R. Yao, T. Chanda, and J. Zakrzewski, Nonergodic dynamics in disorder-free potentials, *Ann. Phys.* **435**, 168540 (2021).
- [32] T. M. Gunawardana and B. Buča, Dynamical l-bits and persistent oscillations in stark many-body localization, *Phys. Rev. B* **106**, L161111 (2022).
- [33] G. Zisling, D. M. Kennes, and Y. B. Lev, Transport in Stark many-body localized systems, *Phys. Rev. B* **105**, L140201 (2022).
- [34] T. Kohlert, S. Scherg, P. Sala, F. Pollmann, B. Hebbe Madhusudhana, I. Bloch, and M. Aidelsburger, Exploring the regime of fragmentation in strongly tilted fermi-hubbard chains, *Phys. Rev. Lett.* **130**, 010201 (2023).
- [35] S. Scherg, T. Kohlert, P. Sala, F. Pollmann, B. Hebbe Madhusudhana, I. Bloch, and M. Aidelsburger, Observing non-ergodicity due to kinetic constraints in tilted fermi-hubbard chains, *Nat. Commun.* **12**, 4490 (2021).
- [36] S. Moudgalya, A. Prem, R. Nandkishore, N. Regnault, and B. A. Bernevig, Thermalization and its absence within Krylov subspaces of a constrained Hamiltonian, *Memorial Volume for Shoucheng Zhang*, 147–209 (WORLD SCIENTIFIC, 2021).
- [37] S. Pai, M. Pretko, and R. M. Nandkishore, Localization in fractonic random circuits, *Phys. Rev. X* **9**, 021003 (2019).
- [38] V. Khemani, M. Hermele, and R. Nandkishore, Localization from Hilbert space shattering: From theory to physical realizations, *Phys. Rev. B* **101**, 174204 (2020).
- [39] S. Moudgalya, B. A. Bernevig, and N. Regnault, Quantum many-body scars and Hilbert space fragmentation: a review of exact results, *Rep. Prog. Phys.* **85**, 086501 (2022).
- [40] G. Francica and L. Dell’Anna, Hilbert space fragmentation in a long-range system, *Phys. Rev. B* **108** (2023).
- [41] P. Brighi, M. Ljubotina, and M. Serbyn, Hilbert space fragmentation and slow dynamics in particle-conserving quantum east models, *SciPost Phys.* **15**, 093 (2023).
- [42] M. Will, R. Moessner, and F. Pollmann, Realization of Hilbert space fragmentation and fracton dynamics in 2d (2023). 2311.05695.
- [43] P. Sala, T. Rakovszky, R. Verresen, M. Knap, and F. Pollmann, Ergodicity breaking arising from Hilbert space fragmentation in dipole-conserving Hamiltonians, *Phys. Rev. X* **10**, 011047 (2020).
- [44] T. Rakovszky, P. Sala, R. Verresen, M. Knap, and F. Pollmann, Statistical localization: From strong fragmentation to strong edge modes, *Phys. Rev. B* **101**, 125126 (2020).
- [45] S. Moudgalya and O. I. Motrunich, Hilbert space fragmentation and commutant algebras, *Phys. Rev. X* **12**, 011050 (2022).
- [46] S. Nandy, J. Herbrich, Z. Lenarčič, A. Głódkowski, P. Prelovšek, and M. Mierzejewski, Emergent dipole moment conservation and subdiffusion in tilted chains (2023). 2310.01862.
- [47] See Supplemental Material for the details of the numerical algorithm determining LIOMs, the orthogonalization of operators, the spectral statistics of the PH model, the simplest extended PH model (with a one additional longer-range pair hopping term), the derivation of effective models of tilted chain and the calculation of subdiffusion from the dynamical structure factor (the density correlation function). Supplemental Material contains Refs. [63–67].
- [48] L. Herviou, J. H. Bardarson, and N. Regnault, Many-body localization in a fragmented Hilbert space, *Phys. Rev. B* **103**, 134207 (2021).
- [49] P. Calabrese, F. H. L. Essler, and G. Mussardo, Introduction to ‘quantum integrability in out of equilibrium systems’, *J. Stat. Mech.* **2016**, 064001 (2016).
- [50] R. M. Nandkishore and M. Hermele, Fractons, *Annu. Rev. Condens. Matter Phys.* **10**, 295 (2019).
- [51] A. Gromov, A. Lucas, and R. M. Nandkishore, Fracton hydrodynamics, *Phys. Rev. Res.* **2**, 033124 (2020).
- [52] A. Głódkowski, F. Peña Benítez, and P. Surówka, Hydrodynamics of dipole-conserving fluids, *Phys. Rev. E* **107**, 034142 (2023).
- [53] K. T. Grosvenor, C. Hoyos, F. Peña-Benítez, and P. Surówka, Space-dependent symmetries and fractons, *Front. Phys.* **9** (2022).
- [54] J. Feldmeier, P. Sala, G. D. Tomasi, F. Pollmann, and M. Knap, Anomalous diffusion in dipole- and higher-moment-conserving systems, *Phys. Rev. Lett.* **125**, 245303 (2020).
- [55] A. Morningstar, V. Khemani, and D. A. Huse, Kinetically constrained freezing transition in a dipole-conserving system, *Phys. Rev. B* **101**, 214205 (2020).
- [56] M. Fremling, Exact gap-ratio results for mixed Wigner surmises of up to 4 eigenvalues (2022). 2202.01090.
- [57] K. Kudo and T. Deguchi, Unexpected non-Wigner behavior in level-spacing distributions of next-nearest-neighbor coupled xxz spin chains, *Phys. Rev. B* **68**, 052510 (2003).
- [58] A. Gubin and L. F. Santos, Quantum chaos: An introduction via chains of interacting spins 1/2, *Am. J. Phys.* **80**, 246–251 (2012).
- [59] M. Long, P. Prelovšek, S. El Shawish, J. Karadamoglou, and X. Zotos, Finite-temperature dynamical correlations using the microcanonical ensemble and the Lanczos algorithm, *Phys. Rev. B* **68**, 235106 (2003).
- [60] P. Prelovšek and J. Bonča, Ground state and finite temperature lanczos methods, *Strongly Correlated Systems - Numerical Methods*, edited by A. Avella and F. Mancini (Springer, Berlin, 2013).
- [61] E. Guardado-Sanchez, A. Morningstar, B. M. Spar, P. T. Brown, D. A. Huse, and W. S. Bakr, Subdiffusion and heat transport in a tilted two-dimensional fermi-hubbard system, *Phys. Rev. X* **10**, 011042 (2020).
- [62] A. Kaczmarek and A. S. Sajna, Slow semiclassical dynamics of a two-dimensional hubbard model in disorder-free potentials, *Phys. Rev. B* **108**, 134304 (2023).
- [63] V. Oganesyan and D. A. Huse, Localization of interacting fermions at high temperature, *Phys. Rev. B* **75**, 155111 (2007).
- [64] Y. Y. Atas, E. Bogomolny, O. Giraud, and G. Roux, Distribution of the ratio of consecutive level spacings in random matrix ensembles, *Phys. Rev. Lett.* **110**, 084101 (2013).
- [65] K. Kudo and T. Deguchi, Level statistics of xxz spin chains with discrete symmetries: Analysis through finite-size effects, *J. Phys. Soc. Jpn.* **74**, 1992 (2005).

- [66] P. Prelovšek, O. S. Barišić, and M. Mierzejewski, Reduced-basis approach to many-body localization, [Phys. Rev. B **97**, 035104 \(2018\)](#).
- [67] J. Herbrych, R. Steinigeweg, and P. Prelovšek, Spin hydrodynamics in the $s = \frac{1}{2}$ anisotropic heisenberg chain, [Phys. Rev. B **86**, 115106 \(2012\)](#).

Supplemental Material: Local integrals of motion in dipole-conserving models with Hilbert space fragmentation

S1. NUMERICAL ALGORITHM DETERMINING LIOMS

A. Details of the algorithm

We focus on a system with L sites, which is described by the Hilbert space with dimension Z spanned by energy eigenstates $H|n\rangle = E_n|n\rangle$. We consider a set of D_O observables $\{A^1, \dots, A^{D_O}\}$ and denote their matrix elements as $A_{nm}^s = \langle n|A^s|m\rangle$. The latter operators are local, traceless and orthonormal with respect to the Hilbert-Schmidt (HS) product introduced in Eq. (1) in the main text, i.e.,

$$\langle A^s A^{s'} \rangle = \frac{1}{Z} \text{Tr}(A^s A^{s'}) = \delta_{ss'}. \quad (\text{S1})$$

Nonergodic systems retain memory of the initial state, so that the correlation function $\lim_{t \rightarrow \infty} \lim_{L \rightarrow \infty} \langle A^s(t) A^s \rangle$ is nonzero for the majority of A^s . This property leads to the nonvanishing stiffness

$$\lim_{\tau \rightarrow \infty} \frac{1}{\tau} \int_0^\tau dt \langle A^s(t) A^s \rangle = \langle \bar{A}^s A^s \rangle = \langle \bar{A}^s \bar{A}^s \rangle = \|\bar{A}^s\|^2, \quad (\text{S2})$$

which equals the squared HS norm of the time-averaged operator, $\bar{A}^s = \sum_{E_n=E_m} A_{nm}^s |n\rangle\langle m|$, see Eq. (3) in the main text. For clarity, we present explicit expressions only for the case with no degeneracies in the many-body spectrum, when $\bar{A}^s = \sum_{n=1}^Z A_{nn}^s |n\rangle\langle n|$.

The nonergodic behavior of operators A^s is encoded in the matrix elements of their time-averaged counterparts \bar{A}^s . Therefore, we build the matrix

$$\mathcal{R} = \begin{bmatrix} A_{11}^1 & A_{11}^2 & \dots & A_{11}^{D_O} \\ A_{22}^1 & A_{22}^2 & \dots & A_{22}^{D_O} \\ \vdots & \vdots & \ddots & \vdots \\ A_{ZZ}^1 & A_{ZZ}^2 & \dots & A_{ZZ}^{D_O} \end{bmatrix}, \quad (\text{S3})$$

which s th column gathers all matrix elements of \bar{A}^s . When degeneracies are present in the many-body spectrum then each row corresponds to a different pair of degenerated energy eigenstates and the number of rows is larger than Z . We also assume that $D_O < Z$, so that the rank of \mathcal{R} is not larger than D_O . Next, we perform the singular value decomposition ($\mathcal{R} = \mathcal{U} \tilde{\Lambda} \mathcal{V}^T$),

$$\mathcal{R}_{ns} = A_{nm}^s = \text{Tr}(|n\rangle\langle n|A^s) = \sum_{\beta=1}^{D_O} \mathcal{U}_{n\beta} \tilde{\lambda}_\beta (\mathcal{V}^T)_{\beta s}, \quad (\text{S4})$$

where the number of non-zero singular values $\tilde{\lambda}_\alpha$ is given by the rank of \mathcal{R} . We take positive $\tilde{\lambda}_\beta$, which are sorted in descending order. Using the orthogonality of matrices \mathcal{U} and \mathcal{V} , we solve Eq. (S4) for the singular values

$$\tilde{\lambda}_\beta \delta_{\beta\beta'} = \text{Tr} \left[\left(\sum_{n=1}^Z \mathcal{U}_{n\beta'} |n\rangle\langle n| \right) \left(\sum_{s=1}^{D_O} \mathcal{V}_{s\beta} A^s \right) \right], \quad (\text{S5})$$

and rewrite the above equation in terms of the Hilbert Schmidt inner product

$$\langle Q^{\beta'} B^\beta \rangle = \frac{\tilde{\lambda}_\beta}{\sqrt{Z}} \delta_{\beta\beta'} \equiv \sqrt{\lambda_\beta} \delta_{\beta\beta'}, \quad (\text{S6})$$

$$Q^\beta = \sqrt{Z} \sum_{n=1}^Z \mathcal{U}_{n\beta} |n\rangle\langle n|, \quad (\text{S7})$$

$$B^\beta = \sum_{s=1}^{D_O} \mathcal{V}_{s\beta} A^s, \quad (\text{S8})$$

cf. Eq. (S1). We have introduced the factor \sqrt{Z} in Eq. (S7) to ensure that the operators Q^β are orthonormal, i.e., $\langle Q^\beta Q^{\beta'} \rangle = \delta_{\beta\beta'}$. We note that the orthogonal transformation of A^s in Eq. (S8) preserves their orthogonality and normalization, i.e., $\langle B^\beta B^{\beta'} \rangle = \delta_{\beta\beta'}$. For clarity, we explicitly account for the norms of operators which appear in Eq. (S6)

$$\langle Q^{\beta'} B^\beta \rangle = \delta_{\beta\beta'} \sqrt{\lambda_\beta} \|Q^{\beta'}\| \|B^\beta\|. \quad (\text{S9})$$

Comparing the above equation with the Cauchy Schwartz inequality one gets $\lambda_\beta \leq 1$ and, most importantly, for $\lambda_\beta = 1$ one obtains $Q^\beta = B^\beta$. All Q^β are conserved by construction, as they are expressed via projectors on eigenstates of the Hamiltonian. We also note that all B^β represent local operators, as they are expressed as linear combinations of local operators A^s . Therefore for $\lambda_\beta = 1$, the operator $Q^\beta = B^\beta$ is both local and conserved, hence it is a LIOM.

While we do not study quasilocal integrals of motion in the present work, we note that they can also be singled out by this procedure. Such operators are not strictly local, but their projections on certain local operators do not vanish in the thermodynamic limit ($L \rightarrow \infty$). From Eq. (S9) one finds that the quasilocal integrals of motion are represented by Q_β for which $0 < \lim_{L \rightarrow \infty} \lambda_\beta < 1$.

B. Relation to the data compression problem and the Mazur bound

The elements of \mathcal{R} in Eq. (S3) store information about the nonergodic behavior of the studied set of operators,

$\{A^1, \dots, A^{D_O}\}$. In general, the rank of \mathcal{R} equals D_O . One may pose a question about a possibility of compressing the data stored in \mathcal{R} . Formally, one looks for a matrix \mathcal{R}^\parallel of a fixed rank $D_L \ll D_O$, which minimizes the Hilbert Schmidt norm $\|\mathcal{R} - \mathcal{R}^\parallel\|$. The solution of this variational problem is given by the Eckart–Young–Mirsky theorem. Namely, the matrix elements of \mathcal{R}^\parallel are given by the same singular value decomposition that we have used for identification of LIOMs,

$$\mathcal{R}^\parallel_{ns} = \sum_{\beta=1}^{D_L} \mathcal{U}_{n\beta} \tilde{\lambda}_\beta (\mathcal{V}^T)_{\beta s}. \quad (\text{S10})$$

In contrast to Eq. (S4), the summation in Eq. (S10) is carried out only over D_L largest singular values. Below, we demonstrate that the data compression via the Eckart–Young–Mirsky theorem is equivalent to the procedure projecting the studied operators onto LIOMs.

Using Eq. (S4), we express the time-averaged operators \bar{A}^s via the conserved operators introduced in Eq. (S7)

$$\begin{aligned} \bar{A}^s &= \sum_{n=1}^Z A^s_{nn} |n\rangle\langle n| = \sum_{\beta=1}^{D_O} \left(\sum_{n=1}^Z \mathcal{U}_{n\beta} |n\rangle\langle n| \right) \tilde{\lambda}_\beta (\mathcal{V}^T)_{\beta s} \\ &= \sum_{\beta=1}^{D_O} Q^\beta \sqrt{\lambda_\beta} (\mathcal{V}^T)_{\beta s} \end{aligned} \quad (\text{S11})$$

$$= \sum_{\beta=1}^{D_O} Q^\beta \langle Q^\beta \bar{A}^s \rangle \quad (\text{S12})$$

In the last step, we have used the relation $\langle Q^\beta \bar{A}^s \rangle = \sqrt{\lambda_\beta} (\mathcal{V}^T)_{\beta s}$, which can be established from \bar{A}^s given by Eq. (S11) and the orthogonality condition $\langle Q^\beta Q^{\beta'} \rangle = \delta_{\beta\beta'}$. Finally, the identity relation for the time-averaged operators $\langle Q^\beta \bar{A}^s \rangle = \langle \bar{Q}^\beta A^s \rangle = \langle Q^\beta A^s \rangle$ allows us to rewrite Eq. (S12) in the following form

$$\bar{A}^s = \sum_{\beta=1}^{D_O} \langle Q^\beta A^s \rangle Q^\beta. \quad (\text{S13})$$

One may repeat the reasoning from Eqs. (S11)-(S13) taking into account only D_L largest singular values. Within such modified procedure we obtain the following operators

$$\bar{A}^{s\parallel} = \sum_{\beta=1}^{D_L} Q^\beta \sqrt{\lambda_\beta} (\mathcal{V}^T)_{\beta s} = \sum_{\beta=1}^{D_L} \langle Q^\beta A^s \rangle Q^\beta, \quad (\text{S14})$$

whose matrix elements are stored in the compressed matrix \mathcal{R}^\parallel , i.e., $\langle n | \bar{A}^{s\parallel} | n \rangle = \mathcal{R}^\parallel_{ns}$. Therefore, the solution of the data compression problem for the matrix \mathcal{R} is equivalent to the projection of the studied operators on LIOMs with $\lambda_\beta = 1$ and (depending on the choice of D_L) on other conserved operators with the largest projections (λ_β), see Eq. (S6).

The Mazur bound [18, 19] for the stiffnesses introduced in Eq. (S2) can be easily obtained from Eq. (S13) together with the orthogonality condition $\langle Q^\beta Q^{\beta'} \rangle = \delta_{\beta\beta'}$,

$$\langle \bar{A}^s \bar{A}^s \rangle = \sum_{\beta=1}^{D_O} \langle Q^\beta A^s \rangle^2 \geq \sum_{\beta=1}^{D_L} \langle Q^\beta A^s \rangle^2. \quad (\text{S15})$$

Finally, we note that the stiffness of operators B^β defined in Eq. (S8) has a particularly simple form. Using Eqs. (S13) and (S6), one arrives at

$$\begin{aligned} \bar{B}^\beta &= \sum_{s=1}^{D_O} \mathcal{V}_{s\beta} \bar{A}^s = \sum_{s=1}^{D_O} \mathcal{V}_{s\beta} \sum_{\beta'=1}^{D_O} \langle Q^{\beta'} A^s \rangle Q^{\beta'} \\ &= \sum_{\beta'=1}^{D_O} \langle Q^{\beta'} \left(\sum_{s=1}^{D_O} \mathcal{V}_{s\beta} A^s \right) \rangle Q^{\beta'} \\ &= \sum_{\beta'=1}^{D_O} \langle Q^{\beta'} B^\beta \rangle Q^{\beta'} = \sqrt{\lambda_\beta} Q^\beta. \end{aligned} \quad (\text{S16})$$

The Hilbert-Schmidt norm is, thus, given by $\|\bar{B}^\beta\|^2 = \lambda_\beta$. If $\lambda_\beta = 1$, then the operator B^β has no off-diagonal matrix elements that are eliminated by the time-averaging and $\|\bar{B}^\beta\| = \|B^\beta\| = 1$. Therefore, we reach the same conclusion as from Eq. (S6), i.e., if $\lambda_\beta = 1$ then the operator B^β is a LIOM.

The most demanding part of numerical implementation of the above algorithm concerns the construction of the matrix \mathcal{R} . In order to single out the matrix elements of time-averaged operators one needs to carry out diagonalization of the studied Hamiltonian. In the case of spin ($s = 1/2$) systems (or spinless fermions) one is typically restricted to systems containing $L \sim 20$ sites.

S2. ORTHOGONALIZATION OF OPERATORS

In order to orthogonalize the set of operators O^j with $j \in \{1, \dots, D_O\}$, it is necessary to construct their traceless counterparts

$$\underline{Q}^j = O^j - c(j), \quad (\text{S17})$$

where $c(j)$ is a real constant fixed by the condition $\text{Tr}(\underline{Q}^j) = 0$. Next, we build the matrix of the Hilbert-Schmidt products

$$R = \begin{bmatrix} \langle \underline{Q}^1 \underline{Q}^1 \rangle & \langle \underline{Q}^1 \underline{Q}^2 \rangle & \dots & \langle \underline{Q}^1 \underline{Q}^D \rangle \\ \langle \underline{Q}^2 \underline{Q}^1 \rangle & \langle \underline{Q}^2 \underline{Q}^2 \rangle & \dots & \langle \underline{Q}^2 \underline{Q}^D \rangle \\ \vdots & \vdots & \ddots & \vdots \\ \langle \underline{Q}^D \underline{Q}^1 \rangle & \langle \underline{Q}^D \underline{Q}^2 \rangle & \dots & \langle \underline{Q}^D \underline{Q}^D \rangle \end{bmatrix}, \quad (\text{S18})$$

which is real and symmetric, and we solve the eigenproblem

$$R = U D U^T, \quad (\text{S19})$$

where \mathcal{D} is a diagonal matrix, $(\mathcal{D})_{ii'} = \sigma_i \delta_{ii'}$, with dimension $D_O \times D_O$ and positive eigenvalues σ_i . The matrix U with dimension $D_O \times D_O$ determines the orthogonal transformation of operators, so that

$$A^i = \frac{1}{\sqrt{\sigma_i}} \sum_{j=1}^{D_O} U_{ji} \underline{Q}^j \quad (\text{S20})$$

are orthogonal and normalized

$$\begin{aligned} \langle A^i A^{i'} \rangle &= \frac{1}{\sqrt{\sigma_i} \sqrt{\sigma_{i'}}} \sum_{j,j'=1}^{D_O} U_{ji} \langle \underline{Q}^j \underline{Q}^{j'} \rangle U_{j'i'} \\ &= \frac{\sigma_{i'}}{\sqrt{\sigma_i} \sqrt{\sigma_{i'}}} \sum_j U_{ji} U_{j'i'} = \delta_{ii'}. \end{aligned} \quad (\text{S21})$$

We emphasize that if O^j are local then A^i inherit this property.

S3. SPECTRAL STATISTICS

A popular measure of quantum chaos is the statistics of the spacings $\delta_i = E_i - E_{i-1}$ between the nearest energy levels E_i and E_{i-1} . In order to avoid the spectral unfolding, it is convenient to study the ratio

$$\tilde{r}_i = \frac{\min(\delta_{i+1}, \delta_i)}{\max(\delta_{i+1}, \delta_i)}, \quad (\text{S22})$$

which is restricted to the interval $[0, 1]$. Energy levels within each symmetry sector of ergodic systems are correlated and experience level repulsion, so that the distribution of ratios \tilde{r} agrees with the prediction of the Gaussian orthogonal ensemble,

$$P_{\text{GOE}}(\tilde{r}) = \frac{27}{4} \frac{\tilde{r} + \tilde{r}^2}{(1 + \tilde{r} + \tilde{r}^2)^{5/2}}, \quad (\text{S23})$$

which vanishes in the limit $\tilde{r} \rightarrow 0$, while its mean is $\langle \tilde{r} \rangle_{\text{GOE}} \approx 0.536$ [63, 64]. Simultaneously, energy levels of nonergodic systems, characterized by an extensive number of LIOMS, can be massively degenerated. If this is not the case, then energy levels are uncorrelated and the distribution of ratios \tilde{r} agrees with the Poisson distribution,

$$P_{\text{P}}(\tilde{r}) = \frac{2}{(1 + \tilde{r})^2}, \quad (\text{S24})$$

which is nonzero in the limit $\tilde{r} \rightarrow 0$, while its mean is $\langle \tilde{r} \rangle_{\text{P}} \approx 0.386$ [63, 64].

We have verified that there are many degeneracies in the spectrum of the PH model (not shown). Following Ref. [36] and [48], we lift these degeneracies by adding a minor disorder to the pair hopping and onsite potential, which preserves the Krylov structure of the Hilbert space.

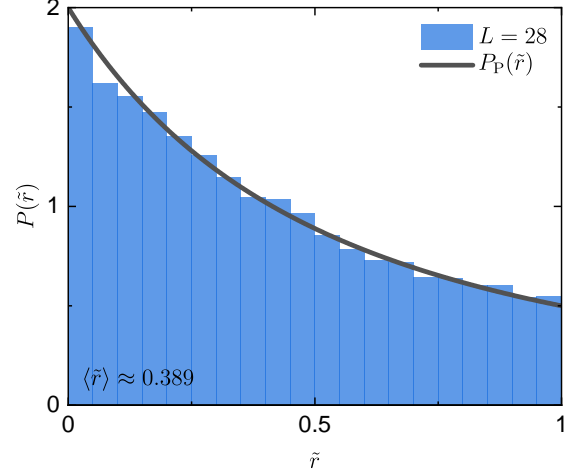


FIG. S1. The spectral statistics of the PH model from Eq. (S25) with $L = 28$ sites. We consider the largest symmetry sector with a fixed dipole moment $M = \frac{L(L+1)}{4} = 203$ and sublattice particle number $n_{\text{even}} = \frac{L}{4} = 7$, which dimension is $\tilde{Z} = 417540$. The histogram has been calculated out of 2000 energy eigenstates in the middle of the spectrum and averaged over 20 Hamiltonian realizations. The solid line corresponds to the Poisson distribution from Eq. (S24).

Specifically, we consider a modified Hamiltonian, which can be written as

$$\tilde{H}_1 = \sum_{i=1}^{L-3} t_i (c_i^\dagger c_{i+3}^\dagger c_{i+2} c_{i+1} + \text{H.c.}) + \sum_{i=1}^L \epsilon_i c_i^\dagger c_i, \quad (\text{S25})$$

where t_i and ϵ_i are identically distributed random numbers drawn from intervals $[0.99, 1.01]$ and $[-0.01, 0.01]$, respectively. In Fig. S1, we present the spectral statistics of \tilde{H}_1 from Eq. (S25) with $L = 28$ sites. We consider the largest symmetry sector with the dipole moment $M = \frac{1}{Z} \text{Tr}(M) = \frac{L(L+1)}{4} = 203$ and sublattice particle number $n_{\text{even}} = \frac{1}{Z} \text{Tr}(n_{\text{even}}) = \frac{L}{4} = 7$, which dimension is $\tilde{Z} = 417540$. The histogram of ratios \tilde{r} has been evaluated in the middle of the spectrum from 2000 energy eigenstates and averaged over 20 realizations of $\{t_i\}$ and $\{\epsilon_i\}$. We observe a remarkable agreement with the Poisson distribution from Eq. (S24) with the mean ratio $\langle \tilde{r} \rangle \approx 0.389$. This is a clear evidence that the PH model from Eq. (S25) supports additional integrals of motion beyond M and n_{even} , which are not fixed in the studied symmetry sector [65]. The latter observation goes in line with the general conclusion of the main text concerning the presence of LIOMS.

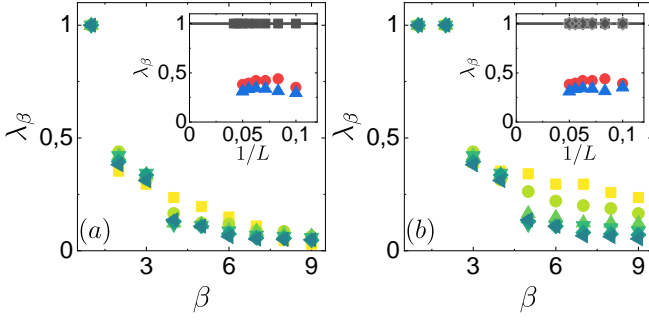


FIG. S2. The norms λ_β for \tilde{H}_2 from Eq. (S26), which is the simplest extension of the PH model. Results are presented for $\beta \leq 9$, $L = 10, \dots, 20$ and various sets of operators: (a) $A^i \in \mathcal{N}$ and (b) $A^i \in \tilde{\mathcal{N}}_{2E}$. The insets show the finite size scalings of the largest λ_β .

S4. HAMILTONIAN FROM EQ. (5) WITHOUT THE LAST TERM

The simplest extension of the PH model is

$$\tilde{H}_2 = H_1 + \sum_{i=1}^{L-4} (c_i^\dagger c_{i+4}^\dagger c_{i+3} c_{i+1} + \text{H.c.}), \quad (\text{S26})$$

where H_1 corresponds to the Hamiltonian from Eq. (4) in the main text. For this model, we have calculated the HS norms λ_β , where B^β are linear combinations of $A^i \in \mathcal{N}$, which are site occupations. The results of numerical calculations are presented in Fig. S2(a). Only one LIOM ($\lambda_1 = 1$) can be observed and it represents the dipole moment M (not shown). Moreover, we have considered an extended set $\tilde{\mathcal{N}}_{2E}$, which includes all operators from \mathcal{N} as well as the pair hopping terms $c_i^\dagger c_{i+3}^\dagger c_{i+2} c_{i+1} + \text{H.c.}$ and $c_i^\dagger c_{i+4}^\dagger c_{i+3} c_{i+1} + \text{H.c.}$ This allows to construct \tilde{H}_2 as a linear combination of $A^i \in \tilde{\mathcal{N}}_{2E}$, see Fig. S2(b). In this case, one obtains two LIOMs that represent the Hamiltonian and the dipole moment. However, the available data do not allow to rule out the possibility that for other λ_β one gets $0 < \lim_{L \rightarrow \infty} \lambda_\beta < 1$. The latter may be interpreted as a presence of additional integrals of motion, which cannot be entirely expressed as linear combinations of operators from the studied set but have nonvanishing projections on operators belonging to this set. Such conserved quantities do not need to be local, e.g., they can be quasilocal in a sense of Ref. [12].

S5. DERIVATION OF EFFECTIVE MODELS OF TILTED CHAIN

The derivation of the PH model, Eq. (4), has been performed so far by the Schrieffer-Wolff transformation of the original Stark model, Eq. (6), assuming large fields $F \gg t$. Specifically, the nearest-neighbor hopping term has been eliminated and the lowest order terms in

the expansion in the strength of t/F have been kept [36]. The effective model conserves by construction the dipole moment M . In general, such procedure can be extended to establish higher order terms, as the ones in the EPH model, Eq. (5). However, one can choose an alternative way and assume weak interactions $V \lesssim F, t$. Then, one can rewrite the Hamiltonian, Eq. (6), within the basis of non-interacting Stark single-particle states, i.e.,

$$H_0 = \sum_j \epsilon_j a_j^\dagger a_j, \quad c_i^\dagger = \sum_j \alpha_{ij} a_j^\dagger, \quad (\text{S27})$$

where (neglecting the boundary effects) energies are equidistant $\epsilon_{j+1} = \epsilon_j + F$ and wave functions are localized $\alpha_{ij} = f(j-i)$ in a range $|j-i| \lesssim t/F$. The interaction term in this basis becomes

$$H' = V \sum_i n_i n_{i+1} = V \sum_{ijklm} \chi_{jk}^{lm} a_l^\dagger a_m^\dagger a_k a_j, \quad (\text{S28})$$

$$\chi_{jk}^{lm} = \sum_i \alpha_{il} \alpha_{i+1,m} \alpha_{i+1,k} \alpha_{ij}. \quad (\text{S29})$$

Such an approach has been previously used in the analysis of an analogous MBL problem [66], where the basis of Anderson single-particle states is the relevant one.

One can classify the terms in H' by the number of sites involved, i.e., H'_2, H'_3, H'_4 . Note that

$$H'_2 = 2V \sum_{j < k} (\chi_{jk}^{jk} - \chi_{jk}^{kj}) n_j n_k, \quad (\text{S30})$$

is the Hartree-Fock term conserving M . The most important terms among the remaining ones are those that also conserve M , in particular those that emerge in H'_4 ,

$$H'_{4dr} = \sum_j \zeta_{dr} [a_{j-r}^\dagger a_j^\dagger a_{j+d+r}^\dagger a_{j+d} + \text{H.c.}], \quad (\text{S31})$$

which generate pair hoppings of different range $r \geq 1$ and distance $d \geq 1$. Keeping only $\tilde{H}'_4 = \sum_{d,r \geq 1} H'_{4dr}$ results in the model containing terms of infinite range. Still, ζ_{dr} decay with $d, r \gg 1$ for large fields $F \gtrsim V$. This allows constructing extensions of the PH model, as the ones from Eqs. (S26) and (5). In principle, one could consider also remaining $H'_4 \neq \tilde{H}'_4$ and H'_3 and eliminate them by an appropriate Schrieffer-Wolff transformation. However, the generated terms would be of a higher order in the interaction, V^m with $m \geq 2$.

S6. SUBDIFFUSION FROM DYNAMICAL STRUCTURE FACTOR

The transport (diffusion) properties of the selected models at $T \rightarrow \infty$ can be studied via the dynamical structure factor (the density correlation function)

$$S(q, \omega) = \frac{1}{\pi} \text{Re} \int_0^\infty dt e^{i\omega t} \langle n_q(t) n_{-q} \rangle, \quad (\text{S32})$$

with

$$n_q = \frac{1}{\sqrt{L}} \sum_i \cos(q(i - L/2)) n_i. \quad (\text{S33})$$

The particle number is conserved, so the dynamical structure factor in the low- q, ω regime should take the hydrodynamic form (see, e.g., [67])

$$S(q, \omega) \sim \frac{1}{\pi} \frac{\chi_q^0 \Gamma_q}{\omega^2 + \Gamma_q^2}, \quad \chi_q^0 = \int d\omega S(q, \omega), \quad (\text{S34})$$

with the relaxation rate $\Gamma_q \sim Dq^z$ where $z > 0$, the corresponding susceptibility $\chi_q^0 = \langle n_q n_{-q} \rangle \sim \chi^0 \sim (1/2)\bar{n}(1 -$

$\bar{n})$ and the particle density $\bar{n} = N/L$.

Results for $S(q, \omega)$ in the EPH model, Eq. (5), were obtained with the micro-canonical Lanczos method (MCLM) [59, 60]. Since the EPH model conserves both the particle number N and the dipole moment M , we performed calculations in the largest symmetry sector with $N = L/2$ and $M = 0$, reaching the system size $L = 32$ with the Hilbert space dimension $N_{st} \sim 10^7$. To obtain high-enough frequency resolution $\delta\omega \sim 4.10^{-4}$, we had to use a large number of Lanczos steps $N_L \sim 5.10^4$.

In Fig. 2(c), we present results for $S(q, \omega)$ for two lowest nonzero $q = 2m\pi/L$ with $m = 1, 2$. The main conclusion is that the numerical results confirm the subdiffusive scaling with $z = 4$ in the low- q, ω regime, since $\pi S(q, \omega \sim 0) = \chi^0/\Gamma_q \sim \chi^0/(Dq^4)$.